IEEE Photonics Journal
An IEEE Photonics Society Publication

Open Access

Copper-Graphene-Based Photonic Crystal Fiber Plasmonic Biosensor

Volume 8, Number 1, February 2016

Ahmmed A. Rifat
G. Amouzad Mahdiraji
Rajib Ahmed
Desmond M. Chow
Y. M. Sua
Y. G. Shee
F. R. Mahamd Adikan

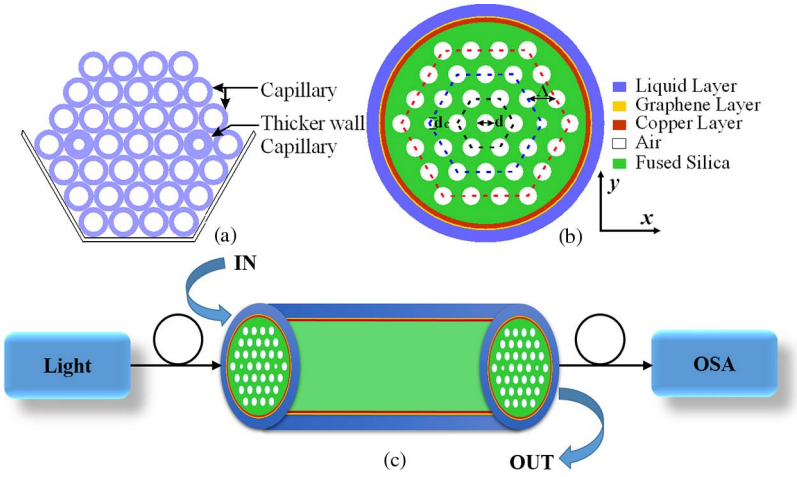

DOI: 10.1109/JPHOT.2015.2510632
1943-0655

IEEE photonics SOCIETY

IEEE

Copper-Graphene-Based Photonic Crystal Fiber Plasmonic Biosensor

Ahmmed A. Rifat,[1] G. Amouzad Mahdiraji,[1] Rajib Ahmed,[2] Desmond M. Chow,[1] Y. M. Sua,[1] Y. G. Shee,[1] and F. R. Mahamd Adikan[1]

[1]Integrated Lightwave Research Group, Department of Electrical Engineering, Faculty of Engineering, University of Malaya, 50603 Kuala Lumpur, Malaysia
[2]Nanotechnology Laboratory, School of Mechanical Engineering, University of Birmingham, Birmingham B15 2TT, U.K.

DOI: 10.1109/JPHOT.2015.2510632

Manuscript received October 29, 2015; revised December 13, 2015; accepted December 16, 2015. Date of publication December 21, 2015; date of current version January 4, 2016. This work was fully supported by the University of Malaya MOHE-High Impact Research under Grant UM.0000005/HIR. C1. Corresponding author: F. R. Mahamd Adikan (e-mail: rafiq@um.edu.my).

Abstract: We propose a photonic crystal fiber surface plasmon resonance biosensor where the plasmonic metal layer and the sensing layer are placed outside the fiber structure, which makes the sensor configuration practically simpler and the sensing process more straightforward. Considering the long-term stability of the plasmonic performance, copper (Cu) is used as the plasmonic material, and graphene is used to prevent Cu oxidation and enhance sensing performance. Numerical investigation of guiding properties and sensing performance is performed by using a finite-element method. The proposed sensor shows average wavelength interrogation sensitivity of 2000 nm/refractive index unit (RIU) over the analyte refractive indices ranging from 1.33 to 1.37, which leads to a sensor resolution of 5×10^{-5} RIU. Due to the simple structure and promising results, the proposed sensor could be a potential candidate for detecting biomolecules, organic chemicals, and other analytes.

Index Terms: Photonic crystal fiber, surface plasmon resonance, optical fiber sensors, optical sensing and sensors.

1. Introduction

Surface plasmon resonance (SPR) is the collective oscillation of free electrons on metal-dielectric interface arising from incident electro-magnetic wave. Resonance occurs when the frequency of incoming photons and surface electrons are matched. At this resonance condition, a sharp loss peak appears and an unknown analyte could be detected by observing the variation of loss peak [1], [2]. Over the past few decades, SPR sensing technique has attracted much attention due to its highly sensitive property. SPR sensors have shown huge potentials in medical diagnostics, bio-molecular analyte detection, organic chemical detection, chemical detection, etc. [3], [4]. SPR sensors require a metallic component carrying large amounts of free electrons. These free electrons provide the real part of a negative permittivity, which is essential for plasmonic materials. Nevertheless, metals are chemically active and prone to oxidization. Oxidization tendency, material losses and corrosion are important factors that weaken the plasmonic property [5]. Generally, gold (Au) and silver (Ag) are widely used as a plasmonic material for SPR sensors [5], [6]. Gold is chemically stable in many environments (aqueous environment, etc.) and shows large resonance

peak shift. However, it has a broad resonance peak, which reduces the accuracy of analyte detection and it is lossy [7], [8]. On the contrary, the utmost conductive material, silver, shows lower loss and sharper resonance peak compared to the other plasmonic materials. However, silver is not chemically stable and could be oxidized easily. Silver film with graphene layer coating could solve the oxidation problem [8], [9]. Due to fast oxidation and degradation properties of silver, silver-graphene is not suitable for long-term plasmonic applications. Recently, Kravets *et al.* experimentally observed that silver-graphene coated plasmonic materials property deteriorates with time. In contrast, copper-graphene coated plasmonic property has shown long-term durability, and its plasmonic performance is more stable, which is over a year [9]. Copper (Cu) is the second most conductive material after silver, and it is much cheaper compared to both gold and silver. Cu material damping rate is the same as Au, and its interband transition is also close to Au [5]. Cu oxidizes easily hence it has not received much attention compared to Au and Ag. However, Cu oxidation could be prevented with graphene layer coating, since graphene is mechanically strong, chemically inert and having hexagonal lattice structure which is impermeable to gas molecules as small as helium and therefore inhibits the penetration of oxygen [10], [11]. Furthermore, graphene coating applied to the metal surface can improve the sensing performance due to the π-π stacking. Besides, it increases the absorption of analyte molecules owing to the high surface to volume ratio and possesses superior plasmonic properties that are suitable for sensing [8]–[10], [12].

Kretschmann set-up is widely used for SPR sensor where the p-polarization or transverse magnetic (TM) light is incident on a prism coated with plasmonic materials (Au, Ag, Cu, etc.) and excites the surface plasmon polaritons (SPP) wave [2]. In 1983, Liedberg *et al.* reported SPR sensor for bio-sensing and gas detection for the first time [13]. Although the prism based SPR sensor (Kretschmann set-up) performance is robust, its structural configuration is bulky due to many required optical and mechanical components therefore not suitable for remote sensing [2]. PCF based SPR sensing technique is considered a possible route to miniaturization. PCF has been proven as a good replacement of prism, having smaller footprint, easier system integration and cost effective. By harnessing its advantages such as small size, easier light launching, single mode propagation and ability in controlling evanescent field penetration, PCF turns out to be a promising candidate for SPR sensor. Recently, numerous microstructured fiber based SPR sensors have been reported where thin plasmonic material layers are coated on the inner walls of air-holes and liquid sample is selectively infiltrated inside these air-holes [7], [14]–[16]. However, they are very challenging to be practically implemented. To overcome these difficulties, D-shape PCF SPR sensors were proposed where one side along the fiber is polished and where the plasmonic metal layers and sensing layer are placed on top of the polished surface [17], [18]. However, accurate polishing effort is required to precisely remove a predetermined portion of the PCF. Recently, PCF SPR biosensors are realized by keeping the metallic layer (Au, Ag, etc.) and sensing layer outside the PCF structure where the air-holes with different sizes are introduced and placed at different positions to control the light propagation in specific directions [8], [19], [20]. Nonetheless, fabrication of such irregular PCF geometry is difficult, even with very accurate fiber preform drilling systems.

In this paper, a more realistic and practically simple PCF SPR biosensor is proposed. Copper is utilized in PCF SPR sensor for the first time due to its long-term stable sensing performance and graphene is used to prevent copper oxidation and enhance the sensor performance. Copper-graphene layer and sensing layer are placed outside the fiber structure to eliminate liquid infiltration and metal coating problem. Owing to the external sensing layer, the analyte can be detected by simply flowing it through or dripped on the outer surface of Cu and graphene layers.

2. Structural Design and Numerical Analysis

Cross-sections of the PCF stacked preform and proposed sensor is shown in Fig. 1(a) and (b), respectively. Fig. 1(c) shows the experimental setup of the proposed sensor where light from a supercontinuum source is coupled to the circular PCF structure. A circular sample holder is considered surrounding the PCF structure. Analyte sample IN and OUT is maintained through a

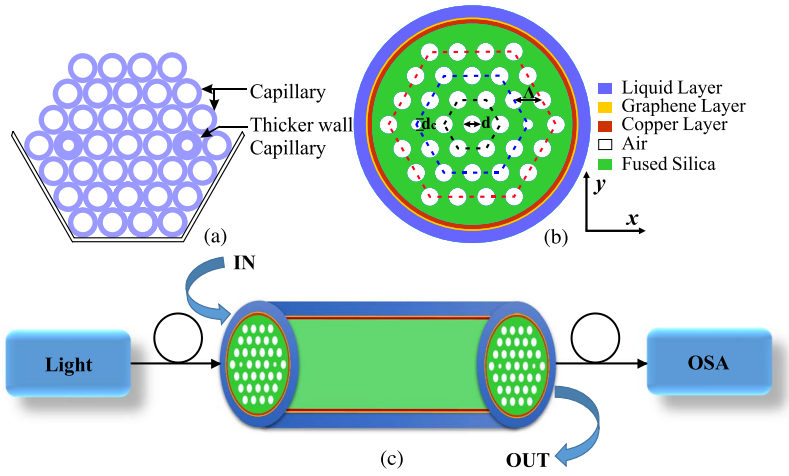

Fig. 1. Cross-section of the proposed (a) PCF's stacked preform, (b) sensor, and (c) schematic diagram of the experimental set-up.

pump. Finally, the transmitted light is coupled to the optical spectrum analyzer (OSA) for the analysis. Considering the central air hole, proposed PCF consists of three hexagonal rings where the air-holes are similar. In the second ring (blue dash line) along the horizontal row of the central hole, the two opposite sides of air-holes are scaled down to allow light propagating through their surrounding silica area. Scaled down holes are placed close to the plasmonic Cu surface to accelerate the excitation of the free electrons. The scaled down air-holes also facilitate coupling of phase-matched core-guided mode and surface plasmon polaritons (SPP) mode. In Fig. 1(b), two adjacent air-holes are placed with uniform distance (pitch size) $\Lambda = 2$ μm, and the air-hole diameter is, $d = 0.50\Lambda$. The scaled down air-holes diameter is $d_c = 0.30\Lambda$. Owing two small air-holes, by introducing thicker wall capillaries, proposed PCF could be fabricated easily by using the standard stack-and-draw method. The refractive index (RI) of fused silica follows Sellmeier equation [7]. Outside the fiber structure, Cu layer of thickness $t = 30$ nm is used. Cu layer could be deposited using electron-beam evaporation method [9]. The complex RI property of Cu has been adopted from [21]. On top of the Cu layer, graphene layer thickness has been calculated by $t_g = 0.34$ nm $\times L$ $(L = 1, 2, 3, \ldots)$, where L is the number of layers. By using transfer printing process and chemical vapor deposition (CVD) process, monolayer or multilayer graphene can be directly grown or deposited on the Cu surface [9], [12]. The complex RI of graphene is determined from the equation $n_g = 3 + iC_1\lambda/3$, where λ is the vacuum wavelength in μm and constant $C_1 \approx 5.446$ μm^{-1} [8]. The fiber structure is surrounded by the analyte to be detected. The guiding properties and the sensing performances are investigated using FEM based commercial software known as COMSOL. Perfectly matched layer (PML) is used as a radiation absorber which absorbs the scattered or radiated light towards the surface. Convergence test also carried out by optimizing the mesh size and PML thickness, which leads to calculate the accurate results.

3. Results and Discussions

PCF SPR sensors performance depends on the evanescent field which is due to light propagation through the core. Stronger modal field is desired to ensure interaction with the sensing layer (analyte) for better sensing performance. The modal analysis of the proposed sensor has been carried out in the *xy*-plane while light is propagating in the *z*-direction. The *y*-component mode is used for the following work due to the larger evanescent field, stronger interaction with the analytes, and higher loss depth as compared to the *x*-component mode. Resonance occurs when the real effective index (n_{eff}) of core-guided mode is matched with the real (n_{eff}) value of SPP mode. At resonance, core-guided mode is coupled to the plasmonic mode, resulting in a

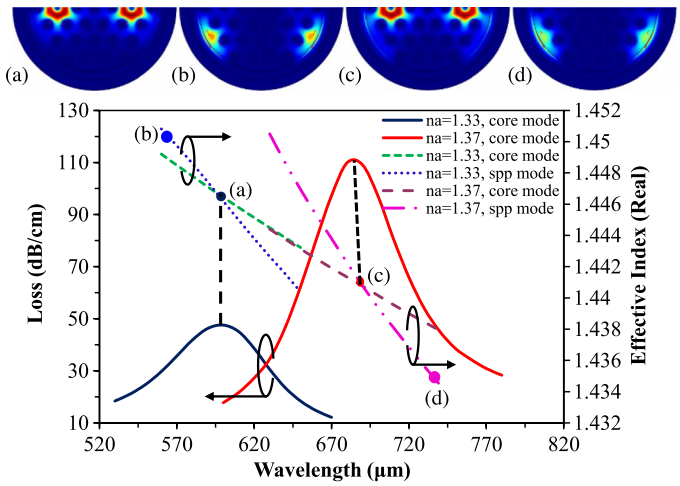

Fig. 2. Dispersion relations of core guided mode (green, maroon), SPP mode (blue, magenta), and loss spectra (black, red). (Inset a, c) Field distribution of the core-guided mode. (Inset b, d) Field distribution of the plasmonic mode for analyte RI $n_a = 1.33$ and 1.37, respectively.

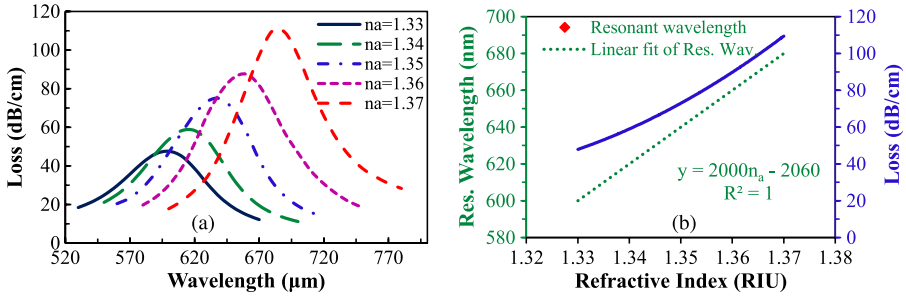

Fig. 3. (a) Fundamental loss spectrum with the variation of analyte RI from 1.33 to 1.37. (b) Linear fit of the resonant wavelength with respect to analyte RI changes ($d_c = 0.30\Lambda$, $d = 0.50\Lambda$, $t = 30$ nm, and $t_g = 0.34$ nm (monolayer)).

sharp loss peak which is called the phase matching point. The phase matching condition of the proposed sensor is shown in Fig. 2. At analyte RI (n_a) 1.33, phase matching is found to be at 600 nm, while at RI 1.37, it shifts towards the longer wavelength and appears at 680 nm wavelength. In Fig. 2, core-guided fundamental mode field distribution is shown in inset (a, c), where the core-mode and plasmonic mode are coupled together. Inset (b, d) of Fig. 2 shows the plasmonic mode field distribution. The phase matching coupling is verified by the coincidence of the resonant peak and the intersection between the dispersion relations of the core-guided mode and SPP mode. The confinement loss is obtained from, $\alpha(\text{dB/cm}) = 8.686 \times (2\pi/\lambda)\text{Im}(n_{\text{eff}}) \times 10^4$, where $\text{Im}(n_{\text{eff}})$ is the imaginary part of effective mode index, and λ is the wavelength in micrometers. Fig. 2 also indicates phase matching wavelength changes with analyte RI. The small change of analyte RI strongly affects $\text{Re}(n_{\text{eff}})$ of the vicinity dielectric-metal surface plasmonic mode and changes the phase matching wavelength. The effect of analyte RI on the loss spectrum is shown in Fig. 3.

In Fig. 3(a), with analyte RI 1.33, resonance peak appears at 600 nm wavelength with the loss depth of 48 dB/cm. Due to the change of analyte RI from 1.33 to 1.37 (with iteration of 0.01), loss peak shifts towards longer wavelengths and loss depth increases simultaneously. Due to increase of analyte RI, the difference between core RI and analyte RI is decreased, which leads to increase of light penetration through the cladding region. Maximum loss depth of 120 dB/cm is

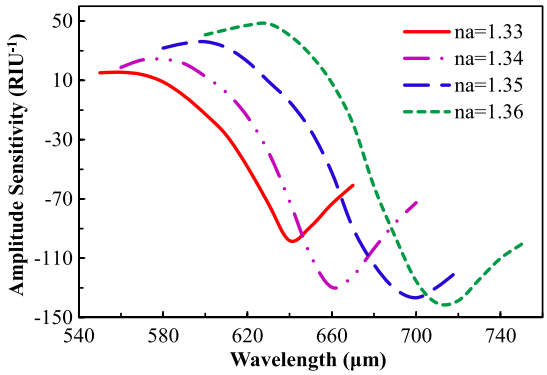

Fig. 4. Amplitude sensitivity spectrum with varying analyte RI 1.33-1.36.

found at resonant wavelength 680 nm when the analyte RI is 1.37, which indicates the maximum energy transferred from the core-guided mode to the SPP mode, resulting in a sharp resonance peak at RI 1.37. In Fig. 3(b) shows the loss peak effects owing to analyte RI changes and also shows the linear resonant wavelength shift where linear regression R^2 is 1. Using the wavelength interrogation method, proposed sensor shows sensitivity and sensor resolution of 2000 nm/RIU and 5×10^{-5} RIU, respectively (by assuming the wavelength resolution is 0.1 nm), which is comparable with the results reported in [16] and [19]. Alternatively, amplitude or phase interrogation sensing scheme could be used, where only measurement at single wavelength is needed for analyte detection. It is simple and cost effective since it does not required spectral manipulation [7], [19]. The amplitude sensitivity is shown in Fig. 4 by varying the analyte RI.

Amplitude sensitivity is given in the following equation [7]:

$$S_A(\lambda)[\text{RIU}^{-1}] = -\frac{1}{\alpha(\lambda, n_a)} \frac{\partial \alpha(\lambda, n_a)}{\partial n_a} \tag{1}$$

where $\partial\alpha(\lambda, n_a)$ is the difference between two adjacent loss spectrum due to a small change in analyte RI. $\alpha(\lambda, n_a)$ is the overall loss, and ∂n_a is the change of analyte RI. The amplitude sensitivity of the proposed sensor increases with higher analyte RI, as shown in Fig. 4. The interaction between evanescent field and plasmon mode increases with the increase of analyte RI. Maximum sensitivity of 140 RIU^{-1} is achieved with analyte RI 1.36, which gives the sensor resolution of 7.1×10^{-5} RIU, considering minimum 1% transmitted intensity can be detected precisely. Additionally, amplitude sensitivities 98, 130, and 137 RIU^{-1} are achieved for the analyte RI of 1.33, 1.34, and 1.35, respectively.

Besides the effects of analyte RI, copper layer thickness also has significant effects on the sensing performance, as shown in Fig. 5. Fig. 5(a) shows the loss value increases with the decrease of Cu thickness and the resonant wavelength is red shifted. However, after surpassing a certain thickness level, as Cu thickness decreases, loss value decreases and exhibits wider resonance curve.

At the analyte RI 1.34, maximum loss value of 48 dB/cm is achieved for Cu thickness of 30 nm at 600 nm wavelength and decreases significantly to 19 dB/cm and resonant wavelength shifts to 630 nm when $t = 50$ nm. By using wavelength interrogation, the sensitivities are 2000, 2000, 1800, and 1500 nm/RIU when the Cu thicknesses are 20, 30, 40, and 50 nm, respectively. Thicker Cu layer introduces more damping which causes the evanescent field penetration towards the surface and the presence of surface plasmons on the sensing layer weakened significantly. The same scenario also observed for amplitude sensitivity, shown in Fig. 5(b). The maximum amplitude sensitivity 98 RIU^{-1} is achieved at 640 nm wavelength when the Cu thickness is 30 nm. When the Cu thickness is increased to 50 nm, amplitude sensitivity decreases gradually to 87 RIU^{-1}, and

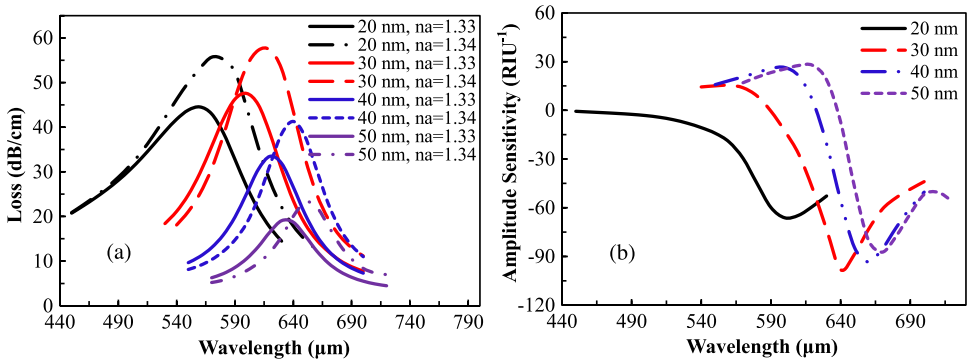

Fig. 5. (a) Loss spectrum and (b) amplitude sensitivity effects with varying Cu thickness 20 to 50 nm ($d_c = 0.30\Lambda$, $d = 0.50\Lambda$, and $t_g = 0.34$ nm).

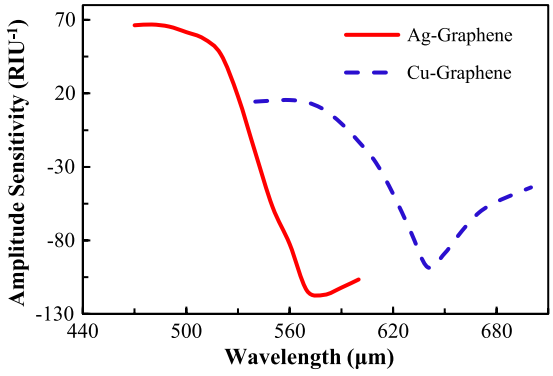

Fig. 6. Comparison of amplitude sensitivity with graphene coated Cu and Ag layer, setting $n_a = 1.33$, $d_c = 0.30\Lambda$, $d = 0.50\Lambda$, $t = t_{Ag} = 30$ nm, and $t_g = 0.34$ nm.

resonant wavelength shifts towards the longer wavelength 670 nm. In contrast, at $t = 20$ nm, sensor shows the amplitude sensitivity of 66 RIU^{-1} with broaden amplitude peak. The maximum amplitude sensitivity leads to sensor resolution of 1×10^{-4} RIU.

Typically, silver has been widely used as a plasmonic material due to its low material losses and sharper resonance peak. As a comparison, amplitude sensitivity for Cu-graphene and Ag-graphene combinations of the proposed sensor is shown in Fig. 6. Ag-graphene and Cu-graphene sensors achieved amplitude sensitivities of 117 and 98 RIU^{-1}, respectively. Although Ag-graphene shows slightly higher amplitude sensitivity as compared to Cu-graphene, yet Cu-graphene combination has even sharper resonance peak with more stable plasmonic performance in the long term [9].

Additionally, graphene has significant effects on sensing performance. Due to its large surface to volume ratio, it interacts with the analytes on the surface resulting in increased sensing performance. The effects of the number of graphene layers on the sensing performance are shown in Fig. 7. In Fig. 7(a), loss depth decreases gradually with the increase of graphene layers and analyte RI. At analyte RI 1.33, the sensor shows red shift of resonant wavelength and the loss value decreases gradually from 48 to 35 dB/cm when thickness of graphene is increased from single layer $(t_g = 0.34 \text{ nm} \times 1)$ to five layers $(t_g = 0.34 \text{ nm} \times 5)$, respectively.

According to Fig. 7(b), amplitude sensitivity also decreases from 98 to 60 RIU^{-1} with the increase of graphene layer from 1 to 5, respectively. Due to damping effect of graphene layer, loss depth and amplitude sensitivity is decreased with the increase of graphene layer thickness. As the graphene is mechanically strong and chemically inert, a single or double layer should be able to prevent the oxidation.

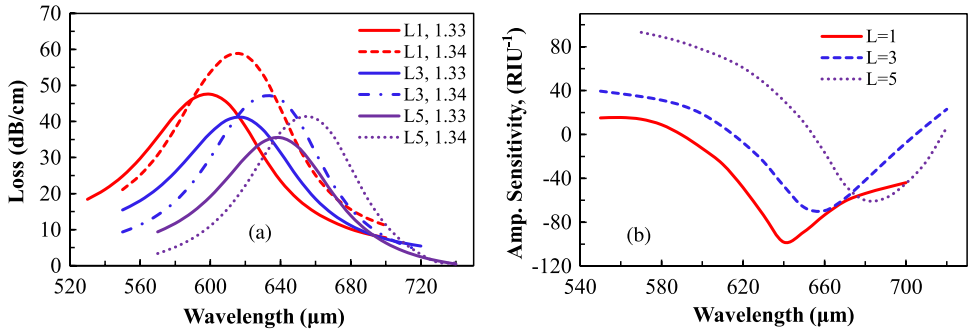

Fig. 7. (a) Loss spectrum and (b) amplitude sensitivity effects with varying the graphene layers from $L = 1$ to 5.

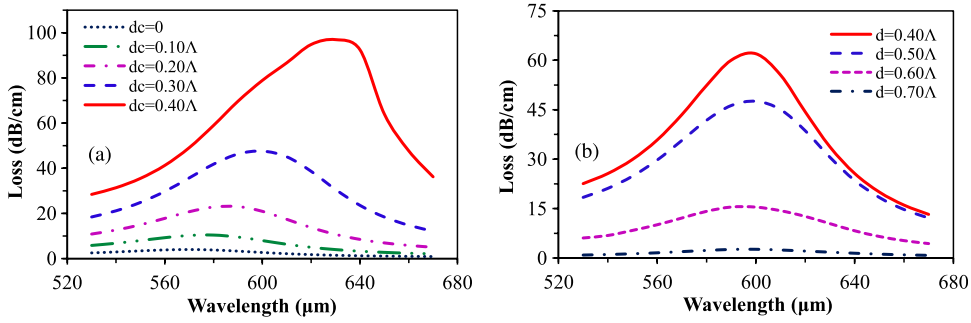

Fig. 8. Loss spectrum with varying (a) scaled-down air-hole diameter d_c and (b) surrounding air-hole diameter d (setting analyte $n_a = 1.33$, $t = 30$ nm, and $t_g = 0.34$ nm).

Further studies have been performed to structural parameters such as scaled-down air-holes diameter (d_c) and the surrounding air-holes diameter (d) to observe the plasmonic excitation (see Fig. 8). Other structural parameters ($t = 30$ nm and $t_g = 0.34$ nm) are kept constant. As shown is Fig. 8(a), loss peaks are shifted towards the longer wavelengths and the loss depths increased gradually as d_c values are increased. The scaled-down air-hole is optimized as $d_c = 0.30\Lambda$. If the diameter is reduced further, light will propagate entirely in the core which will decrease intensity of the evanescent field (which overlaps the metal-dielectric interface). As a result, sensing performance will diminish. If the air-hole diameter d_c is increased, it will reduce the effective index of core. Therefore, it will reduce light guidance along the core and spread out over the cladding region. It also effects on the sensing performance. By considering all issues $d_c = 0.30\Lambda$ is optimized. Fig. 8(b) shows, with increase of outer air-hole size (d), loss peak maintains resonant wavelength 600 nm while the loss depth decreases significantly, which indicates light is more confined in the core. The optimized air-holes diameter d is 0.50Λ. Furthermore, low loss value opens the possibility to work with long-haul fiber optic systems to generate the measurable signal which helps to detect the analytes easily.

4. Conclusion

In summary, a simple, novel Copper-graphene based PCF SPR sensor has been proposed. Guiding properties and sensing performance of the proposed sensor are numerically investigated by FEM. Proposed sensor shows the maximum wavelength interrogation sensitivity of 2000 nm/RIU and achieved the sensor resolution of 5×10^{-5} RIU. Furthermore, it shows the amplitude sensitivity of 140 RIU^{-1} with the sensor resolution 7.1×10^{-5} RIU. The proposed sensor structure is simpler among the reported PCF SPR sensors which could be realized using the standard stack-and-draw fabrication method and the sputtering, CVD deposition method.

References

[1] J. Homola, S. S. Yee, and G. Gauglitz, "Surface plasmon resonance sensors: Review," *Sens. Actuators B, Chem.*, vol. 54, no. 1/2, pp. 3–15, Jan. 1999.

[2] B. Gupta and R. Verma, "Surface plasmon resonance-based fiber optic sensors: Principle, probe designs, and some applications," *J. Sens.*, vol. 2009, 2009, Art. ID 979761.

[3] Y. Zhao, Z.-Q. Deng, and J. Li, "Photonic crystal fiber based surface plasmon resonance chemical sensors," *Sens. Actuators B, Chem.*, vol. 202, pp. 557–567, Oct. 2014.

[4] C. Caucheteur, T. Guo, and J. Albert, "Review of plasmonic fiber optic biochemical sensors: Improving the limit of detection," *Anal. Bioanal. Chem.*, vol. 407, no. 14, pp. 3883–3897, May 2015.

[5] P. R. West *et al.*, "Searching for better plasmonic materials," *Laser Photonics Rev.*, vol. 4, no. 6, pp. 795–808, Nov. 2010.

[6] G. V. Naik, V. M. Shalaev, and A. Boltasseva, "Alternative plasmonic materials: Beyond gold and silver," *Adv. Mater.*, vol. 25, no. 24, pp. 3264–3294, Jun. 2013.

[7] A. Rifat *et al.*, "Photonic crystal fiber-based surface plasmon resonance sensor with selective analyte channels and graphene-silver deposited core," *Sensors*, vol. 15, no. 5, pp. 11499–11510, May 2015.

[8] J. Dash and R. Jha, "Graphene based birefringent photonic crystal fiber sensor using surface plasmon resonance," *IEEE Photon. Technol. Lett.*, vol. 26, no. 11, pp. 1092–1095, Jun. 2014.

[9] V. Kravets *et al.*, "Graphene-protected copper and silver plasmonics," *Sci. Rep.*, vol. 4, 2014, Art. ID 5517.

[10] M. Schriver *et al.*, "Graphene as a long-term metal oxidation barrier: Worse than nothing," *ACS Nano*, vol. 7, no. 7, pp. 5763–5768, Jul. 2013.

[11] J. S. Bunch *et al.*, "Impermeable atomic membranes from graphene sheets," *Nano Lett.*, vol. 8, no. 8, pp. 2458–2462, Aug. 2008.

[12] O. Salihoglu, S. Balci, and C. Kocabas, "Plasmon-polaritons on graphene-metal surface and their use in biosensors," *Appl. Phys. Lett.*, vol. 100, no. 21, May 2012, Art. ID 213110.

[13] B. Liedberg, C. Nylander, and I. Lunström, "Surface plasmon resonance for gas detection and biosensing," *Sens. Actuators*, vol. 4, no. 2, pp. 299–304, Dec. 1983.

[14] D. Gao, C. Guan, Y. Wen, X. Zhong, and L. Yuan, "Multi-hole fiber based surface plasmon resonance sensor operated at near-infrared wavelengths," *Opt. Commun.*, vol. 313, pp. 94–98, Feb. 2014.

[15] Z. Fan *et al.*, "High-sensitivity of refractive index sensor based on analyte-filled photonic crystal fiber with surface plasmon resonance," *IEEE Photon. J.*, vol. 7, no. 3, Jun. 2015, Art. ID 4800809.

[16] J. N. Dash and R. Jha, "SPR biosensor based on polymer PCF coated with conducting metal oxide," *IEEE Photon. Technol. Lett.*, vol. 26, no. 6, pp. 595–598, Mar. 2014.

[17] L. Peng *et al.*, "A surface plasmon biosensor based on a D-shaped microstructured optical fiber with rectangular lattice," *IEEE Photon. J.*, vol. 7, no. 5, pp. 1–9, Oct. 2015.

[18] F. Shi *et al.*, "An elliptical core D-shaped photonic crystal fiber-based plasmonic sensor at upper detection limit," *Plasmonics*, vol. 10, no. 6, pp. 1–6, Dec. 2015.

[19] R. Otupiri *et al.*, "A novel birefringent photonic crystal fibre surface plasmon resonance biosensor," *IEEE Photon. J.*, vol. 6, no. 4, Aug. 2014, Art. ID 6801711.

[20] A. A. Rifat *et al.*, "Surface plasmon resonance photonic crystal fiber biosensor: A practical sensing approach," *IEEE Photon. Technol. Lett.*, vol. 27, no. 15, pp. 1628–1631, Aug. 2015.

[21] A. D. Rakic, A. B. Djurisic, J. M. Elazar, and M. L. Majewski, "Optical properties of metallic films for vertical-cavity optoelectronic devices," *Appl. Opt.*, vol. 37, no. 22, pp. 5271–5283, Aug. 1998.